

Frequency Response Enhancement of Optical Injection-Locked Lasers

Erwin K. Lau, *Member, IEEE*, Hyuk-Kee Sung, *Member, IEEE*, and Ming C. Wu, *Fellow, IEEE*

Abstract—The modulation response of injection-locked lasers has been carefully analyzed, theoretically and experimentally, with a focus on the strong optical injection regime. We derive closed-form solutions to the relaxation oscillation (resonance) frequency and damping term, as well as the low-frequency damping term, and discuss design rules for maximizing resonance frequency and broadband performance. A phasor model is described in order to better explain the enhancement of the resonance frequency. Experimental curves match closely to theory. Record resonance frequency of 72 GHz and broadband results are shown.

Index Terms—Amplitude modulation, frequency response, injection locking, semiconductor lasers.

I. INTRODUCTION

OPTICAL telecommunications systems rely on the conversion of electrical modulation into an optical format. The efficiency of this conversion is of great importance. There are a wide variety of needs; for example, many applications require a large modulation bandwidth, others require high link gain (conversion efficiency), while others require narrowband responses centered at high frequencies [1]–[3]. The injection-locked laser system has been shown to enhance all of these functionalities beyond that of a directly modulated laser [4]–[8]. In order to push the frequency limits of injection-locked laser systems, it is important to understand the physical mechanisms that govern its dynamics. The basic theory has been developed by several groups and can describe a wide array of benefits from the injection-locked laser, including RIN reduction [9]–[15], suppression of nonlinear effects [16]–[18], and relaxation oscillation (RO) frequency enhancement [19]–[23]. Recently, the development of ultrastrong injection locking has greatly enhanced these effects while also introducing special considerations. In this paper, we systematically analyze the established differential equation theory, focusing on the effects of ultrastrong injection on the frequency response. Recently, Wiczorek used bifurcation analysis and explained the effect of the linewidth enhancement factor on the modulation response [24]. Here, our purpose is to simplify the complex rate equations by using a

small-signal approach, in order to bring physically intuitive solutions to each of the features in the frequency response of directly modulated injection-locked laser systems. We discover the physical parameters that dominate the RO (resonance) frequency and also the low-frequency drop-off of ultrastrong injection-locked lasers. We then specify design rules for maximizing resonance frequency and enhancing bandwidth. We discover a new design rule for increasing the bandwidth such that it exceeds the enhanced resonance frequency.

II. THEORY

The most common model for injection-locked lasers uses a set of three differential equations, as published by several authors [25]–[28]. The differential equation governing the complex field of an injection-locked laser is similar to that of a free-running laser, with the addition of an injection term

$$\frac{dE(t)}{dt} = \frac{1}{2}g\Delta N(1 + j\alpha)E(t) + \kappa A_{\text{inj}} - j\Delta\omega_{\text{inj}}E(t) \quad (1)$$

where $E(t)$ is the slave laser's complex field. This model ignores spontaneous emission and noise. This equation can be split into the field magnitude and phase by assuming that $E(t) = A(t)\exp(j\phi(t))$. The split equation, along with the carrier rate equation, constitute the three differential equations of injection-locked lasers [28]

$$\frac{dA(t)}{dt} = \frac{1}{2}g[N(t) - N_{\text{th}}]A(t) + \kappa A_{\text{inj}} \cos\phi(t) \quad (2)$$

$$\frac{d\phi(t)}{dt} = \frac{\alpha}{2}g[N(t) - N_{\text{th}}] - \kappa \frac{A_{\text{inj}}}{A(t)} \sin\phi(t) - \Delta\omega_{\text{inj}} \quad (3)$$

$$\frac{dN(t)}{dt} = J - \gamma_N N(t) - \{\gamma_P + g[N(t) - N_{\text{th}}]\}A(t)^2 \quad (4)$$

where $A(t)$, $\phi(t)$, and $N(t)$ are the slave laser's field magnitude, field phase, and carrier number. $A(t)$ is normalized as $A^2(t) = S(t)$, where $S(t)$ is the photon number. $\phi(t)$ is the phase difference between master and slave: $\phi(t) \equiv \phi_{\text{slave}}(t) - \phi_{\text{master}}$. g , N_{th} , α , J , γ_N , and γ_P are the slave laser's linear gain coefficient, threshold carrier number, linewidth enhancement factor, current, carrier recombination rate, and photon decay rate, respectively. The injection terms, κ , A_{inj} , and $\Delta\omega_{\text{inj}}$ are the coupling rate, injected field magnitude, and detuning frequency, respectively. The detuning frequency is defined as the difference between master and free-running slave frequencies.

Manuscript received July 3, 2007; revised September 10, 2007. This work was supported in part by the Defense Advanced Research Projects Agency (DARPA) aPROPOS program under Contract W911NF-06-1-0269 and the DARPA seedling program on high-speed lasers.

E. K. Lau and M. C. Wu are with the Department of Electrical Engineering and Computer Sciences, University of California, Berkeley, CA 94720-1774 USA (e-mail: elau@eecs.berkeley.edu; wu@eecs.berkeley.edu).

H.-K. Sung is with the School of Electronic and Electrical Engineering Department, Hongik University, Seoul 121-791, Korea (e-mail: hksung@hongik.ac.kr).

Digital Object Identifier 10.1109/JQE.2007.910450

A. Steady State Solutions

Murakami solves the differential equations for the steady-state field magnitude, phase, and carrier number, defined here as A_0 , ϕ_0 , and N_0 , respectively [28]. Solving for the free-running field magnitude, A_{fr} , in (4), we can set the above-threshold carrier number, $\Delta N_0 \equiv N_0 - N_{th}$, to zero, obtaining

$$A_{fr}^2 = \frac{J - \gamma_N N_{th}}{\gamma_P}. \quad (5)$$

Using this and solving for the steady-state values of the injection-locked laser, we obtain

$$A_0^2 = \frac{A_{fr}^2 - \frac{\gamma_N}{\gamma_P} \Delta N_0}{1 + \frac{g \Delta N_0}{\gamma_P}} \quad (6)$$

$$\phi_0 = \sin^{-1} \left\{ -\frac{\Delta \omega_{inj}}{\kappa \sqrt{1 + \alpha^2}} \frac{A_0}{A_{inj}} \right\} - \tan^{-1} \alpha \quad (7)$$

$$\Delta N_0 = -\frac{2\kappa}{g} \frac{A_{inj}}{A_0} \cos \phi_0. \quad (8)$$

The most convenient solution method is to choose a phase value and injection ratio (defined as $R = A_{inj}/A_0$), knowing that the bounds of the phase across the locking range are approximately $\cot^{-1} \alpha$ to $-\pi/2$, from the negative to positive frequency detuning edges, respectively [25]. Knowing ϕ_0 and substituting (8) into (6) yields

$$0 = A_0^3 - \left[\frac{2\kappa}{\gamma_P} A_{inj} \cos \phi_0 \right] A_0^2 - A_{fr}^2 A_0 - \frac{\gamma_N}{\gamma_P} \frac{2\kappa}{g} A_{inj} \cos \phi_0 \quad (9)$$

whose roots, A_0 , can be easily solved by a numerical root-solving program. Then, (8) solves for ΔN_0 and we rearrange (7) to solve for $\Delta \omega_{inj}$

$$\Delta \omega_{inj} = -\kappa \sqrt{1 + \alpha^2} \frac{A_{inj}}{A_0} \sin(\phi_0 + \tan^{-1} \alpha). \quad (10)$$

B. Small-Signal Solutions

The linearized form of (2)–(4) can be placed in matrix form

$$\begin{bmatrix} m_{AA} + s & m_{A\phi} & m_{AN} \\ m_{\phi A} & m_{\phi\phi} + s & m_{\phi N} \\ m_{NA} & 0 & m_{NN} + s \end{bmatrix} \begin{bmatrix} \Delta A \\ \Delta \phi \\ \Delta N \end{bmatrix} = \begin{bmatrix} 0 \\ 0 \\ \Delta J \end{bmatrix} \quad (11)$$

where the matrix terms are

$$\begin{aligned} m_{AA} &= z \cos \phi_0 \\ m_{A\phi} &= z A_0 \sin \phi_0 \\ m_{AN} &= -\frac{1}{2} g A_0 \\ m_{\phi A} &= \frac{-z \sin \phi_0}{A_0} \\ m_{\phi\phi} &= z \cos \phi_0 \\ m_{\phi N} &= -\frac{\alpha}{2} g \\ m_{NA} &= 2A_0 (\gamma_P - 2z \cos \phi_0) \\ m_{NN} &= \gamma_N + g A_0^2 \end{aligned} \quad (12)$$

TABLE I
INJECTION-LOCKED LASER PARAMETERS

Symbol	Value	Units
λ	1550	nm
g	5667	1/s
N_{th}	2.214×10^8	#
α	3	-
J	$2.6 \times J_{th}$	1/s
J_{th}	2.1×10^{17}	1/s
γ_N	1	1/ns
γ_P	333	1/ns
L	500	cm
r	0.3	-
κ	183	1/ns

where $z \equiv \kappa A_{inj}/A_0$. The magnitude of the frequency response is then

$$H(s) \equiv \frac{\Delta A}{\Delta J} = M \frac{s + Z}{s^3 + As^2 + Bs + C} \quad (13)$$

where

$$\begin{aligned} A &= m_{AA} + m_{\phi\phi} + m_{NN} \\ B &= m_{AA}m_{\phi\phi} + m_{AA}m_{NN} + m_{\phi\phi}m_{NN} \\ &\quad - m_{A\phi}m_{\phi A} - m_{AN}m_{NA} \\ C &= m_{AA}m_{\phi\phi}m_{NN} + m_{A\phi}m_{\phi N}m_{NA} \\ &\quad - m_{A\phi}m_{\phi A}m_{NN} - m_{AN}m_{NA}m_{\phi\phi} \\ Z &= \frac{(m_{A\phi}m_{\phi N} - m_{AN}m_{\phi\phi})}{m_{AN}} \\ M &= -m_{AN}. \end{aligned} \quad (14)$$

Therefore, the frequency response can be easily determined by (13) and its auxiliary equations.

In order to elucidate the trends found in (13), we simulate the frequency response for different values of detuning frequency and injection ratio. Table I lists the parameters used in the simulations in this paper, unless otherwise noted. Using the steady-state solutions found in (6)–(10) and the small-signal response in (12)–(14), we can plot the state variables across the locking range map, as shown in Fig. 1. From Fig. 1(a), we see that the positive frequency detuning edge is described by the smallest phase. Fig. 1(b) shows that the resonance frequency increases with detuning and injection ratio. Fig. 1(c) shows that, at the positive edge of the locking range, the field starts at its free-running value at the positive detuning edge and for low injection ratios. It increases with decreasing detuning and higher injection ratios. Fig. 1(d) shows that the carrier density is at threshold on the positive edge of the detuning range. It gradually decreases with decreasing detuning and increasing injection ratio. The regions marked as “n.s.” signifies the unstable locking regime [29]–[31]. This demonstrates that the resonance frequency, internal field, and carrier number deviate only at strong injection ($R > -10$ dB) regimes.

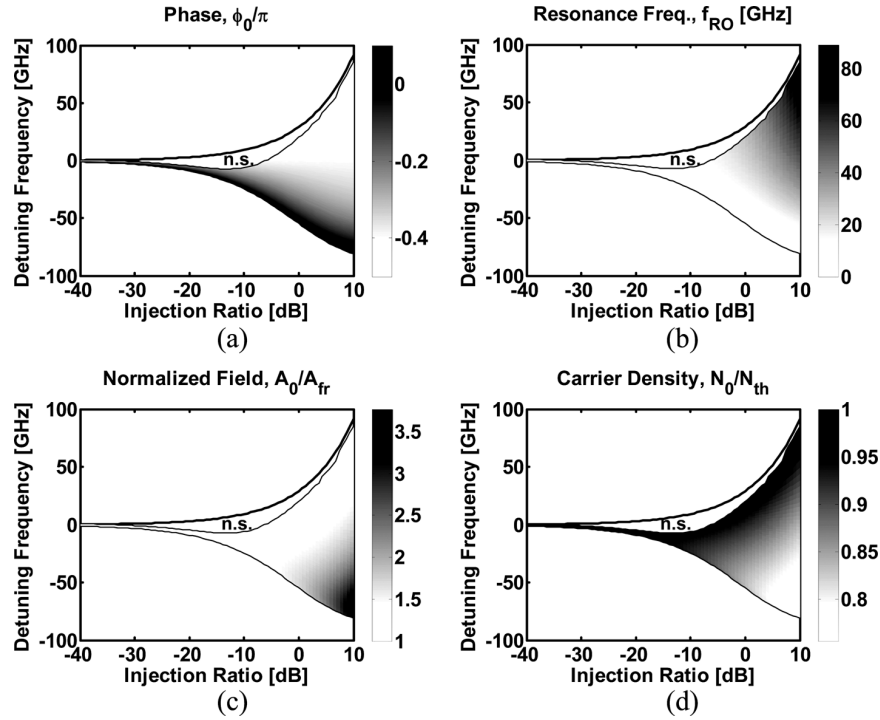


Fig. 1. Locking map versus (a) phase, (b) resonance frequency, (c) normalized field, and (d) normalized carrier density.

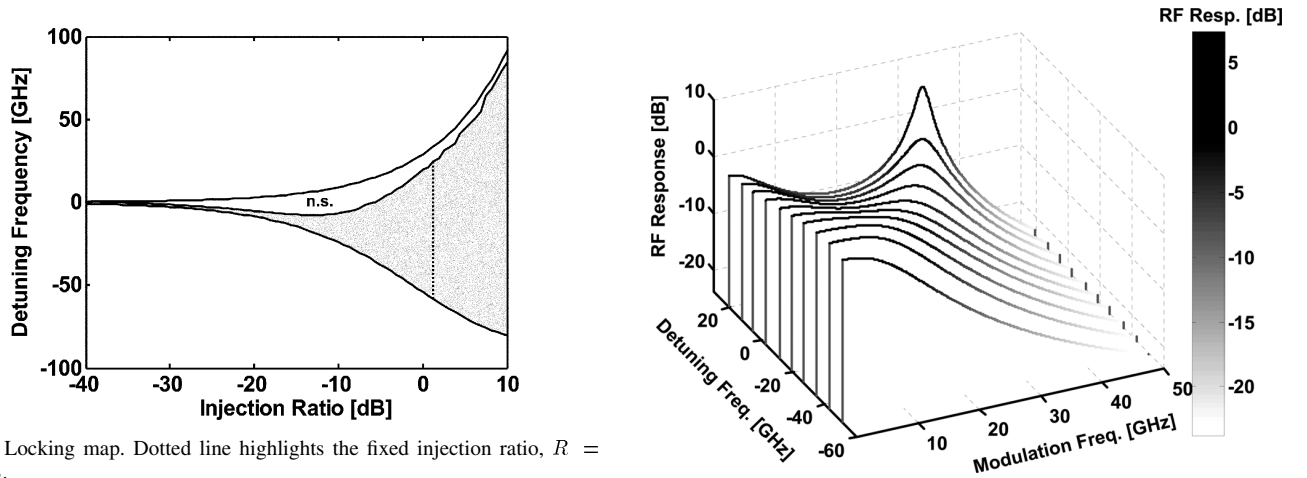


Fig. 2. Locking map. Dotted line highlights the fixed injection ratio, $R = 1.25$ dB.

If we plot the frequency response shown in (13) for fixed injection ratio across the detuning range, as shown in the dotted line in Fig. 2, we obtain a family of frequency response curves, as shown in Fig. 3. Note that the resonance peak is enhanced as the detuning frequency increases. Additionally, the low-frequency gain for the negatively detuned curves is higher than the free-running gain, and will be discussed in Section II-E. These regimes are experimentally described in greater detail in [8]. Fig. 4 shows the accompanying pole/zero diagram of the injection-locked system. Note that it is a single-zero, three-pole system. The two complex conjugate poles determine the resonance frequency. As the detuning increases, the poles' imaginary parts increase in magnitude while their real parts decrease. This causes an enhanced resonance frequency and decreased damping, as described in Section II-C and D, respectively. As also can be seen in Fig. 3, the response between dc and resonance for the positive detuning cases “dips” down quite dramatically. This is a large factor in determining the 3-dB bandwidth

Fig. 3. Theoretical waterfall plot showing frequency response versus detuning, for fixed injection ratio, $R = 1.25$ dB, normalized to dc free-running response. The slices represent frequency response curves across the dotted line in Fig. 2.

of these positively detuned cases. The cause of the dip is discussed in Section II-F.

C. Resonance Frequency

The concept of resonance frequency enhancement by injection locking has been known for a decade [5], [26], [32]. The two major parameters that affect the resonance frequency are injection ratio and frequency detuning. The determinant of the frequency response can be used to determine the resonance frequency

$$D(s) = s^3 + As^2 + Bs + C. \\ = (s + \omega_P)(s - j\omega_R + \frac{1}{2}\gamma)(s + j\omega_R + \frac{1}{2}\gamma) \quad (15)$$

The roots of this equation will be a pair of complex conjugate roots, $\pm j\omega_R - \gamma/2$, and a real, negative root, $-\omega_P$. As with a

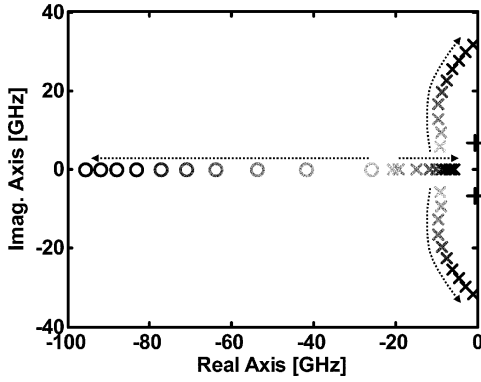


Fig. 4. Pole/zero diagram across detuning range of Fig. 2, for $R = 1.25$ dB. There are 2 complex conjugate poles, 1 real pole, and 1 real zero. Solution is stable if poles remain in the negative real region. Arrows indicate direction of increasing detuning frequency. The sets of poles and zeros correspond to the frequency response slices shown in Fig. 3. The 2 plus marks indicate the complex conjugate poles of the free-running laser.

free-running laser, the imaginary part of the complex conjugate pair gives us the resonance frequency. We can approximate this value as follows.

To find the resonance frequency, we look for the complex roots of the determinant, D . For resonance frequencies in the gigahertz range and above, the last term, C , can be neglected

$$C \ll s^3, As^2, Bs. \quad (16)$$

In this range, the value of C only affects the magnitude of the resonance peak, not its frequency. Solving for a pure driving frequency

$$D(j\omega) \approx j\omega(B - \omega^2 + j\omega A). \quad (17)$$

The determinant is proportional to that of a classic damped oscillator and takes the form

$$D(j\omega) \propto j\omega(\omega_R^2 - \omega^2 + j\gamma\omega) \quad (18)$$

where the resonance frequency ω_R is

$$\omega_R^2 \approx B \quad (19)$$

and whose damping γ is

$$\gamma \approx A. \quad (20)$$

The first three terms of B , shown in (14), contain only diagonal matrix terms in (11) and are typically weak. Therefore, under typical conditions, we can consider the last two nondiagonal terms in B to dominate, yielding

$$\omega_R^2 \approx -m_{AN}m_{NA} - m_{A\phi}m_{\phi A}. \quad (21)$$

The first term is the resonance attributed to the photons and carriers

$$\begin{aligned} -m_{AN}m_{NA} &= g\gamma_P A_0^2 \left(1 + \frac{g}{\gamma_P} \Delta N_0\right) \\ &= \omega_{R0}^2 \left(1 - \frac{\gamma_N}{\gamma_P} \frac{\Delta N_0}{A_{fr}^2}\right) \end{aligned} \quad (22)$$

where $\omega_{R0} = (g\gamma_P A_{fr}^2)^{1/2}$ is the relaxation oscillation of the free-running laser, using the equality in (6). The second term in (22) is much smaller than unity and therefore $-m_{AN}m_{NA} \approx \omega_{R0}^2$. Using (12) and (22) to expand (21), we get

$$\omega_R^2 \approx \omega_{R0}^2 + \Delta\omega_R^2 \quad (23)$$

where we have defined the resonance frequency enhancement term as the second term in (21)

$$\Delta\omega_R = \sqrt{-m_{A\phi}m_{\phi A}} = \left| \kappa \frac{A_{inj}}{A_0} \sin \phi_0 \right|. \quad (24)$$

which describes the resonance enhancement attributed to the photon field and phase coupling. The steady-state condition of (3) is

$$-\frac{\alpha}{2}g(N_0 - N_{th}) + \Delta\omega_{inj} + \kappa \frac{A_{inj}}{A_0} \sin \phi_0 = 0. \quad (25)$$

Using (24) and (25), we obtain a more physical formula

$$\Delta\omega_R = \left| -\frac{\alpha}{2}g(N_0 - N_{th}) + \Delta\omega_{inj} \right|. \quad (26)$$

As described by Murakami, the resonance frequency enhancement is equal to the difference between the master laser frequency and that of the slave laser's natural cavity mode frequency [28]. This cavity mode is shifted by α via the first term in (26). Equation (23) is similar to Henry's formulation [26], but derived differently. It also improves upon Murakami's approximate formula [28], which does not include the absolute value sign and also approximates the resonance frequency as zero for negative detuning frequencies or small injection ratios, when the frequency enhancement is small. In these two regimes, (23) reduces to the original free-running resonance frequency, which is closer to experiment. When the enhancement is much larger than the free-running resonance frequency, the total resonance frequency approximates to the enhancement term, $\Delta\omega_R$.

The implications of (26) is that the resonance frequency is roughly proportional to the detuning frequency. In fact, it will tend to be larger by the α -parameter enhancement. The larger the detuning, the larger the resonance frequency will become. The limit to the resonance frequency is proportional to the mode spacing. Since this paper focuses on a single-mode theory of the slave laser, the effects of multiple modes has not been taken in account. Practically, if the master laser detunes far enough away from the primary mode such that it approaches the frequency of an adjacent slave mode, it will lock to the adjacent mode. Hence, the practical limit to the frequency detuning will be a function of the mode spacing of the slave laser. The larger the spacing, the larger the potential resonance frequency enhancement. For a Fabry–Perot laser, this may only be 100 GHz, whereas a DFB could be > 200 GHz and a vertical-cavity surface-emitting laser (VCSEL) even larger. Therefore, it is important to either suppress adjacent modes or increase the free-spectral range of the Fabry–Perot laser cavity. With proper laser cavity engineering, the resonance frequency can be made to be several hundreds of gigahertz.

D. Damping of the Enhanced Resonance

Here, we describe an approximate term for the damping coefficient. This is useful for describing the gain of the resonance peak. We can expand the damping term, using (12), (14), and (20)

$$\gamma \approx \gamma_N + gA_0^2 + 2z \cos \phi_0. \quad (27)$$

Using the steady-state solution for (2), we can replace the second term on the right-hand side (RHS) to a more physical term

$$\gamma \approx \gamma_0 - g(N_0 - N_{\text{th}}) \quad (28)$$

where $\gamma_0 = \gamma_N + gA_0^2$ is the free-running damping term. Therefore, the injection-locked laser's damping is the free-running damping, enhanced by the reduction of gain below threshold. The injection-locked laser resonance is primarily due to energy oscillating between the slave field and the slave phase interfering with the injected master light. The reduced gain allows a portion of this oscillating energy to be lost to the carriers. We can make an analogy to a *RLC* circuit oscillator, where the field, phase, and carriers are the energy in the capacitor, inductor, and heat lost through the resistor. The capacitor and inductor energies oscillate between each other, while increasing the resistance causes more energy to be leaked into heat, thus damping the oscillations.

Equation (28) is accurate if C is negligible. In the previous section, this was a suitable approximation, when we only needed to find the frequency of resonance. However, when modulated with frequencies near the resonance, the approximate determinant in (18) becomes small and C becomes important in determining the magnitude of the determinant

$$D(s) = s \left(s + j\omega_R + \frac{1}{2}\gamma \right) \left(s - j\omega_R + \frac{1}{2}\gamma \right) + C. \quad (29)$$

In this case, near resonance, we can assume that the damping at resonance is

$$\begin{aligned} D(j\omega_R) &= j\omega_R \left(j\omega_R + j\omega_R + \frac{1}{2}\gamma \right) \\ &\quad \times \left(j\omega_R - j\omega_R + \frac{1}{2}\gamma \right) + C \\ &\approx j\omega_R (2j\omega_R) \left(\frac{1}{2}\gamma \right) + C \\ &= -\gamma\omega_R^2 + C. \end{aligned} \quad (30)$$

This can be viewed as a modified damping term, where

$$\begin{aligned} -\gamma_M \omega_R^2 &= -\gamma\omega_R^2 + C \\ \gamma_M &= \gamma - \frac{C}{\omega_R^2}. \end{aligned} \quad (31)$$

When the laser is near the positive detuning frequency edge ($\phi = -\pi/2$), the frequency response exhibits a pronounced resonance. Solving for C at this edge, we obtain

$$C \left(\phi = \frac{-\pi}{2} \right) = z\alpha g\gamma_P A_0^2 + z^2 (\gamma_N + gA_0^2). \quad (32)$$

From (24) and the definition of z , we can approximate $z \approx \Delta\omega_R$, so that

$$\gamma_M \left(\phi = \frac{-\pi}{2} \right) \approx -\frac{\alpha g\gamma_P A_0^2}{\Delta\omega_R} - g(N_0 - N_{\text{th}}). \quad (33)$$

The carrier number must be sufficiently below threshold for the damping term to be positive and the solution to remain in the region of convergence.

One important point to note is that as the frequency detuning increases, the model predicts that the damping will approach zero. As the peak gain at resonance increases, the output modulation eventually exceeds the small-signal limit. The small-signal analysis used in this paper would no longer be valid in this strong peak regime. In our experiments, near this point, the two lasers typically become unlocked before the modulation power becomes larger than the free-running slave laser cavity mode.

E. Low-Frequency Gain

The low-frequency modulation response can oftentimes be higher than the free-running response. As shown in Fig. 3, this typically occurs near the negative detuning frequency edge of the locking range, where the resonance frequency is very low. Intuitively, when the laser is near the negative detuning edge, the extremely low resonance frequency contributes to increasing the dc gain. We can derive an analytical formula for this.

At zero frequency, (13) reduces to

$$H(j\omega = 0) = \frac{-m_{AN}m_{\phi\phi} + m_{A\phi}m_{\phi N}}{C}. \quad (34)$$

Expanding this into laser parameters yields (35), shown at the bottom of the page. We know to look for the peak dc response near the negative detuning frequency edge. However, when the system is locked exactly at the negative detuning frequency edge, $\phi_0 = \cot^{-1} \alpha$, which would make the numerator term, $\cos \phi_0 - \alpha \sin \phi_0 = 0$, leading to poor dc response. From this, we deduce that the peak is near, but not at, the negative detuning edge.

When modulation is detected by a photodetector, the modulation sideband beats with the main laser line to determine the magnitude of modulation. Hence, when we calculate the RF response, we must multiply the response, $H(\omega)$, with the dc optical field magnitude, A_0 . This favors the negative detuning side since the field increases above free-running as the system approaches this edge [Fig. 1(c)]. Additionally, we can claim that

$$\gamma_N \ll gA_0^2 \quad (36)$$

$$H(0) = \frac{\frac{1}{2}gzA_0 (\cos \phi_0 - \alpha \sin \phi_0)}{z^2 (\gamma_N + gA_0^2) + gzA_0^2 (\gamma_P - 2z \cos \phi_0) (\cos \phi_0 - \alpha \sin \phi_0)}. \quad (35)$$

since the carrier recombination rate is much slower than the excess above-threshold stimulated emission rate, as long as the laser is sufficiently above threshold. This inequality is further amplified near the negative detuning edge, since the field is again higher than free-running at this edge. This reduces the response to

$$A_0 H(0) = \frac{\frac{1}{2}(\cos \phi_0 - \alpha \sin \phi_0)}{z + (\gamma_P - 2z \cos \phi_0)(\cos \phi_0 - \alpha \sin \phi_0)}. \quad (37)$$

One can solve this function by noting that z depends on R and A_0 , the latter which depends on ϕ_0 . This function is complicated to maximize; however some general trends can be noted. In general, this function is maximized when R is larger, since the response is proportional to A_0 (which is large for negative detuning and larger injection ratios). The function also grows with increasing α and decreasing γ_P .

F. Frequency Response: The Real Pole

The value of the third, real pole factors greatly in the size of the dip between dc and resonance. The smaller the pole's magnitude, the earlier the dip appears in the frequency response, leading to poor 3-dB bandwidth. Here, we attempt to extract some trends for mitigating this effect. Effectively, we wish to maximize the third pole frequency.

The full determinant, when expanded, takes on a value of

$$D(s) = (s + \omega_P) \left(s + j\omega_R + \frac{1}{2}\gamma \right) \left(s - j\omega_R + \frac{1}{2}\gamma \right) \approx s^3 + (\gamma + \omega_P)s^2 + (\omega_R^2 + \gamma\omega_P)s + \omega_R^2\omega_P \quad (38)$$

where ω_P is defined as the value of the third, real pole. Comparing it to the determinant equation in (15), we see that the final term in both equations can be equated, giving us

$$\omega_P \approx \frac{C}{\omega_R^2}. \quad (39)$$

For sufficiently positive detuning and large injection ratios, the resonance frequency easily dominates over the damping value. It is clear that the higher the resonance frequency, the smaller the pole (and therefore, larger dip), which corresponds to the trend seen in the pole/zero diagram shown in Fig. 4 and the frequency response curves in Fig. 3.

We approximate C as being dominated by the second and third terms in (14): $m_{A\phi}m_{\phi N}m_{NA} - m_{A\phi}m_{\phi A}m_{NN}$. Since the pole is approximately C/ω_R^2 from (39), and by using the fact that $\omega_R^2 \approx -m_{A\phi}m_{\phi A}$, we can approximate the pole as being simply

$$\begin{aligned} \omega_P &\approx m_{NN} - \frac{m_{A\phi}m_{\phi N}m_{NA}}{\omega_R^2} \\ &= \gamma_N + \left(1 - \frac{\alpha\gamma_P\kappa\sqrt{R}\sin\phi_0}{\omega_R^2} \right) gS_0. \end{aligned} \quad (40)$$

The carrier recombination rate is small and therefore (40) is dominated by the last term, and is proportional to the stimulated recombination rate. This causes a low-frequency drop-off that is proportional to the stimulated recombination rate. Physically,

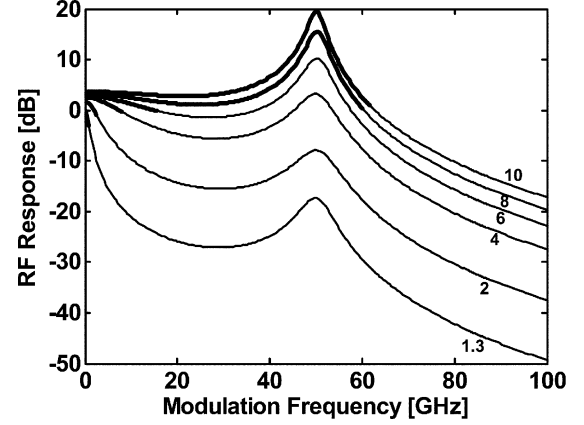


Fig. 5. Frequency response of OIL for various bias conditions, for a constant value of injection ratio and resonance frequency ($R = 4$, $f_{RO} = 50$ GHz). The lines correspond to different current bias levels in units of multiples of threshold current $[J/J_{th}]$. The bold portions correspond to the response within the 3-dB frequency.

this can be interpreted as the carrier injection rate is no longer directly coupled to the relaxation oscillation dynamics, which now correspond to the resonance created by energy exchange between the slave field amplitude and phase. This is in contrast to a free-running laser, whose carrier injection rate is directly coupled to the free-running RO dynamics, which corresponds to the resonance created by energy exchange between carriers and photons. Hence, while the free-running laser exhibits increased carrier injection rates proportional to the RO frequency, the injection-locked laser injection rates are limited, in part, by the stimulated recombination rate, which is on the order of a few GHz, even when enhanced by the increased stimulated emission of the laser cavity. Mainly, the most effective way to increase this is to increase the photon density of the cavity by increased bias current, as shown in Fig. 5, or by negative detuning (since the photon density rises with negative detuning). In Fig. 5, we show the effect of the photon density on the frequency response. We fix the RO frequency at 50 GHz and increase the bias current. The values of the real pole frequencies are: 0.8, 2.7, 7.8, 12.9, 17.8, and 22.7 GHz for the bias conditions $1.3 \times$, $2 \times$, $4 \times$, $6 \times$, $8 \times$, and $10 \times J_{th}$, respectively. Here, we see that the 3-dB bandwidth can be extended to beyond the resonance frequency only when the real pole has been enhanced to sufficiently high frequencies. The bias conditions for $8 \times J_{th}$ and above result in 3-dB responses > 60 GHz.

G. Frequency Response: The Zero

The zero of the frequency response solution in (13) is

$$Z = \frac{(m_{AN}m_{\phi\phi} - m_{A\phi}m_{\phi N})}{m_{AN}}. \quad (41)$$

After expanding this with (12) and reducing, the zero's value is simply

$$Z = z(\alpha \sin \phi_0 - \cos \phi_0). \quad (42)$$

Hence, across the detuning range, from the negative to positive edges, the zero takes on a value of $Z = 0$ to $Z = -z\alpha$. In terms of optimizing the bandwidth of the frequency response, the zero

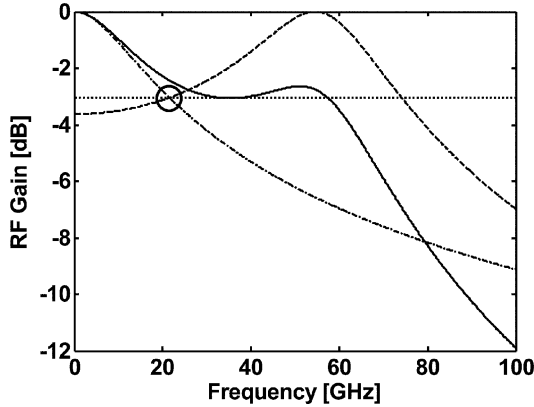


Fig. 6. Graphic representation of method for maximizing bandwidth. The dash-dot line corresponds to the response of the real pole. The dashed line corresponds to the response of the resonance frequency. The 3-dB point (dotted line) of both lines must meet to maximize the total bandwidth, shown as the solid line.

should be minimized, so that once the modulation frequency exceeds the zero's value, the numerator will scale roughly with the modulation frequency. This corresponds to bias points close to the negative detuning edge. Unfortunately, the zero scales with injection ratio, which is necessary for increasing bandwidth. Fortunately, a large zero frequency doesn't hurt the modulation bandwidth, since the numerator looks like a constant for modulation frequencies much smaller than the zero frequency. A small zero value would only serve to mitigate the effects of the dip caused by the third (real) pole. The approximate optimal point would be when the zero value equals the third pole value, thereby canceling the effect of both. This would leave an approximately two-pole system, which we know from classic laser physics does not dip before hitting the resonance frequency. However, this point would correspond to a very low resonance frequency, and would gain scant benefits from the enhanced resonance. Otherwise, reducing the α parameter may serve to reduce the zero. Still, the effect of lowering the third pole is more dominant than reducing the value of the zero.

H. Optimizing Bandwidth

The broadband regime, as explained in [8] is a delicate balance between the dc-to-resonance dip, the damping factor, and the resonance frequency. In general, these values are complex analytical functions. Although it is difficult to derive an intuitive analytical formula to assist in optimization of the injection-locked system for maximum broadband performance, we can make some general observations and trends. As stated in Section II-F, the bias current, injection ratio, and photon decay rate should be increased.

We can estimate the maximum bandwidth point (across the detuning range) by following a few approximations. The dip, caused by the real pole, should not go 3 dB below dc before the modulation frequency reaches the 3-dB bandwidth determined by the 2 complex poles of the resonance frequency. The intersection of these two points, shown as circled in Fig. 6, represents this condition. The resonance frequency is then the approximate maximum bandwidth point.

Taking into consideration the zero and the real pole, we attempt to find its 3-dB point by solving for the circled point in Fig. 6

$$\left| \frac{j\omega_{3dB} - Z}{j\omega_{3dB} - P} \right|^2 = \frac{Z^2}{2P^2} \quad (43)$$

which yields

$$\omega_{3dB} = \frac{PZ}{\sqrt{Z^2 - 2P^2}}. \quad (44)$$

The 3-dB bandwidth of the 2-pole resonance peak (dashed) is simply $\omega_R - (\gamma/2)$. Setting these two points equal yields

$$\omega_R - \frac{\gamma}{2} = \frac{PZ}{\sqrt{Z^2 - 2P^2}}. \quad (45)$$

One can numerically solve for the ϕ_0 that will satisfy this equation. This yields the approximate bandwidth as simply ω_R .

Although there is no specific quantitative condition of injection ratio or detuning frequency that will determine the maximum bandwidth point, we can draw some conclusions. First, the real pole frequency must be maximized. This can be done by reducing the detuning frequency, increasing the injection ratio, and increasing the photon density (via bias current). Second, the RO frequency can be increased, but not too far beyond the frequency of the real pole. Increasing the RO frequency can be accomplished by increasing the injection ratio or detuning frequency. Third, the RO damping must be sufficiently small enough to enhance the response reduction caused by the real pole, but not too small that the resonance enhancement is too narrowband that the real pole fall-off is not sufficiently enhanced. Hence, the detuning frequency should be somewhere in the middle of the locking range. It is important to reiterate that simply increasing the injection ratio and detuning frequency will increase the RO frequency, but the bandwidth will eventually be limited by the real pole frequency. Therefore, as stated above, increasing the photon density (via bias current) and/or injection ratio are the best ways to increase the 3-dB response.

I. Phasor Diagram

Substituting into the complex field rate equation, (1), yields

$$\frac{dE(t)}{dt} = \frac{1}{2}g\Delta NE(t) + \kappa A_{inj} - j\Delta\omega E(t) \quad (46)$$

where we have included the shift of the cavity mode with the frequency detuning term and $\Delta\omega$ is simply a signed version of (26)

$$\Delta\omega \equiv \omega_{inj} - \omega_{cav} = -\frac{\alpha}{2}g(N_0 - N_{th}) + \Delta\omega_{inj}. \quad (47)$$

Henry developed a phasor diagram model for injection-locked lasers that shows the effects of injected light on the slave field [26]. In Fig. 7, we introduce a phasor diagram that shows the mechanisms to achieve a steady-state injection-locked system. The phasor is in the frame-of-reference of the master laser frequency. Therefore, if the slave were lasing at the master laser frequency, the phasor would be static and would not rotate with time. To be locked, we desire the dynamic phasor vectors to sum

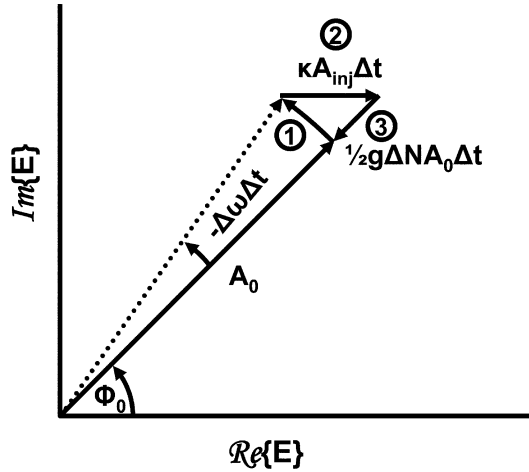


Fig. 7. Phasor model for injection locking, showing phasor perturbation in a time interval, Δt . Vector 1 corresponds to the free-running slave angular rotation, with respect to the frame-of-reference of the master laser frequency. Vector 2 is the vector addition of the injected master light at phase ϕ . Vector 3 is the reduction in amplitude due to the reduced gain.

to zero, resulting in a slave laser that is locked to the master. The angle of the phasor is the phase between master and slave $\phi(t)$. However, the slave, even when locked, will lase at a frequency $\Delta\omega$ away from the master, and therefore will rotate $\Delta\omega\Delta t$ in a time interval Δt as shown in the last term in (46) and in vector 1 of Fig. 7. Since the injected master laser light has a phase equal to 0 in this frame-of-reference, the injected term is represented as a real vector, as shown in the second term on the RHS of (46) and in vector 2. Finally, the gain must reduce to lower the amplitude so that the slave field will return to steady-state, shown in the first term of the RHS of (46) and vector 3.

This clearly shows that, despite being injection-locked, the slave continues to lase at its cavity mode frequency. The injected light serves to continually shift the phase of the slave so that it appears to lase at the frequency of the master. Therefore, frequency-filtering effects of the slave's mirrors or laser structure (within the single-mode regime) will not affect the theory as we detune the master away from the slave. This allows us to use the same theory for Fabry-Perots, distributed feedback lasers (DFBs), distributed Bragg reflectors (DBRs), and VCSELs alike.

III. EXPERIMENT

In this section, we attempt to verify the theory via experiments. The experimental setup is shown in Fig. 8. The slave laser used for the experiments was a 1550-nm capped-mesa buried heterostructure DFB laser [33]. The length was 500 μm , width was 1 μm , and a threshold of 8 mA and was typically biased to 3.5 times threshold. The grating strength, κL (grating coupling coefficient times laser length), was 3–4. The laser was heat-sunk and temperature controlled at 289 K. The master laser (SDL 8610) was amplified by an erbium-doped fiber amplifier (EDFA) made by Calmar Optcom. The polarization is matched to the slave laser via a polarization controller (PC). A circulator is used to ensure isolation between slave output and master input. The slave output is sent to either an optical spectrum analyzer (OSA) or a photodetector followed by an electrical spectrum analyzer (ESA). In order to measure frequencies above 50 GHz (the limit

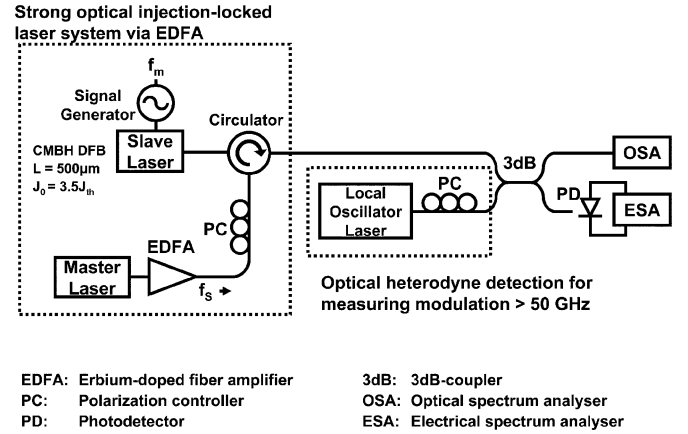


Fig. 8. Experimental optical injection locking setup with optional heterodyne detection.

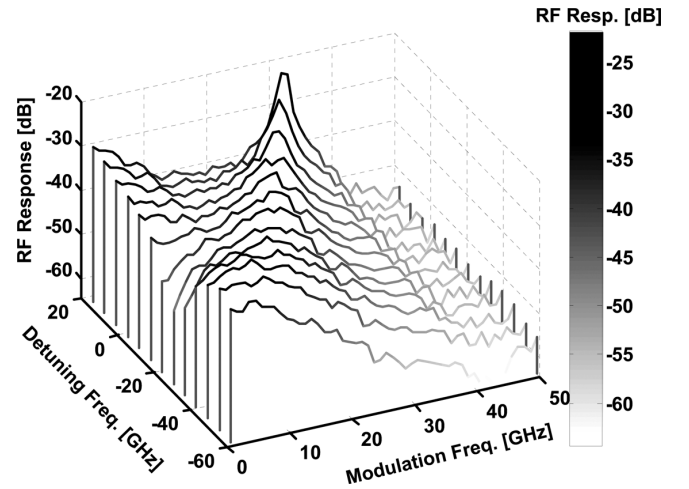


Fig. 9. Experimental waterfall plots showing frequency response versus detuning, for $R = 8$ dB.

of our direct detection setup), we used a heterodyne detection scheme [34]. When using direct detection, the local oscillator is simply turned off.

A. Resonance Frequency Evolution

Fig. 6 shows the experimental frequency response across the frequency detuning range. The waterfall plot shows a family of frequency responses from $\Delta f = -60$ GHz to $+20$ GHz. The injection ratio was fixed at $R = +8$ dB. The enhancement of the resonance frequency can be easily seen as the frequency detuning increases, starting from a few GHz at the negative detuning edge to 34 GHz at the positive detuning edge. The three selected frequency responses of Fig. 8 show the three regimes of modulation, as explained in [8]. Fig. 9 is in good agreement with the theoretical curves calculated in Fig. 3. The injection ratios are different due to the difficulties of measuring the exact injection ratio within the actual slave laser cavity. Nevertheless, the general trends are consistent, as are the quantitative resonance frequency evolution.

Fig. 10 experimentally shows the resonance frequency dependence on detuning and injection ratio, demonstrating the theory described in Fig. 1(b). The trend for increasing the resonance frequency is apparent when increasing the frequency detuning and/or injection ratio.

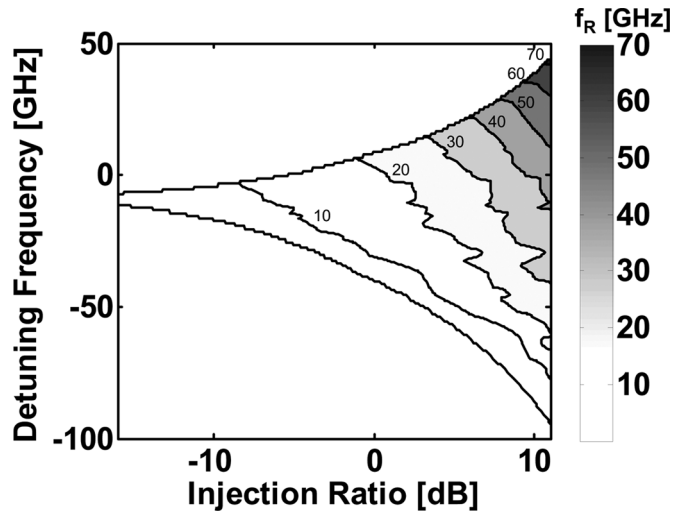


Fig. 10. Experimental mapping of resonance frequency versus locking map parameters (injection ratio and detuning frequency).

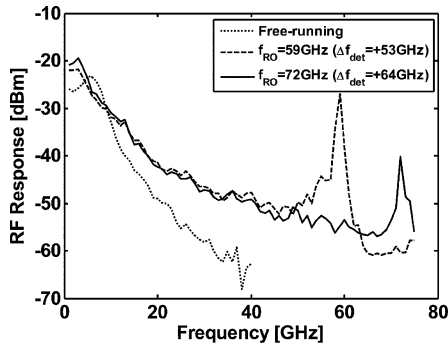


Fig. 11. Experimental frequency response curve showing resonance frequencies of 59 and 72 GHz. $R = +16$ dB.

B. 72-GHz Resonance Frequency and 44-GHz Broad-band Results

Using the trends of the resonance frequency described in the theory and shown in the experiments above, we optimized the system for achieving the highest resonance frequency possible. A resonance frequency of 72 GHz was obtained and is shown in Fig. 11. Response above 50 GHz was measured by the heterodyne detection technique described in [34]. The results were calibrated for cable loss, photodetector loss, and bias-T loss, but electrical losses above 50 GHz and losses from laser parasitics and microwave probe were not included.

Optimizing for broadband performance, we obtain the results shown in Fig. 12. The 3-dB frequency is 44 GHz. Again, electrical loss and photodetector loss was calibrated, but laser parasitic loss and loss from the microwave probe could not be calibrated.

IV. CONCLUSION

The classic differential equations for injection-locked lasers are used to describe the resonance frequency and damping evolution. Trends for the evolution of RO frequency, field amplitude and phase, and carrier density are shown for different injection ratios and detuning frequencies. A comprehensive study of the pole/zero evolution is performed. Closed-form solutions for the relaxation oscillation frequency and damping, as well as for the low-frequency damping, are described. Trends for

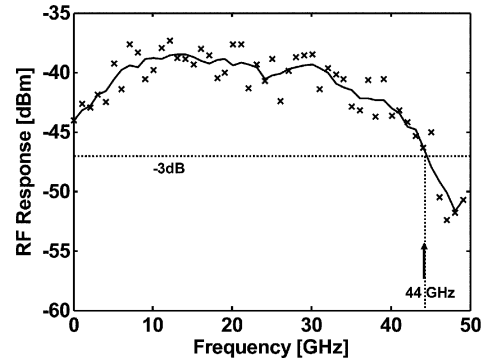


Fig. 12. Experimental frequency response curve showing a broadband, 3-dB response of 44 GHz. $R = +18$ dB, $\Delta f = -60.5$ GHz.

optimizing the relaxation oscillation frequency and bandwidth are discussed. We find that the relaxation oscillation is the root sum square of the free-running slave RO frequency and the injection-locked enhanced resonance frequency. The enhanced resonance frequency is roughly proportional to the frequency detuning between master and slave. The maximum detuning, and, therefore, RO frequency, obtainable is proportional to the frequency spacing between adjacent modes. Lasers with large free spectral ranges (DFBs and VCSELs) can potentially exhibit RO frequencies of several hundreds of gigahertz. We also show that although we can increase the RO frequency, damping typically dominates, causing a narrowband response. Although this may be useful for some applications, we discuss methods of increasing the broadband performance. The bandwidth is ultimately limited by the real pole damping frequency, distinct from the RC parasitics. It can be enhanced by increasing the real pole frequency, notably by increasing the photon density of the slave laser (mainly via the bias current). A phasor model is introduced that explains the coherent dynamics of injection locking. Experimental curves match closely to theory. A record resonance frequency of 72 GHz and broadband response of 44 GHz are shown.

ACKNOWLEDGMENT

The authors would like to thank Prof. C. Chang-Hasnain and X. Zhao of the University of California, Berkeley, and Prof. R. Tucker of the University of Melbourne, Australia, for helpful discussions.

REFERENCES

- [1] A. J. Seeds, "Microwave photonics," *IEEE Trans. Microw. Theory Tech.*, vol. 50, no. 3, pp. 877–887, Mar. 2002.
- [2] Y. Yamamoto, "Receiver performance evaluation of various digital optical modulation-demodulation systems in the 0.5–10 μm wavelength region," *IEEE J. Quantum Electron.*, vol. QE-16, no. 11, pp. 1251–9, Nov. 1980.
- [3] C. H. Cox, III, G. E. Betts, and L. M. Johnson, "An analytic and experimental comparison of direct and external modulation in analog fiber-optic links," *IEEE Trans. Microw. Theory Tech.*, vol. 38, no. 5, pp. 501–509, May 1990.
- [4] T. B. Simpson and J. M. Liu, "Enhanced modulation bandwidth in injection-locked semiconductor lasers," *IEEE Photon. Technol. Lett.*, vol. 9, no. 10, pp. 1322–4, Oct. 1997.
- [5] X. J. Meng, T. Chau, and M. C. Wu, "Experimental demonstration of modulation bandwidth enhancement in distributed feedback lasers with external light injection," *Electron. Lett.*, vol. 34, no. 21, pp. 2031–2031, 1998.

- [6] H. K. Sung *et al.*, "Optical injection-locked gain-lever distributed bragg reflector lasers with enhanced RF performance," in *Proc. IEEE Int. Topical Meeting Microw. Photon.*, Ogunquit, ME, 2004, pp. 225–228.
- [7] H. K. Sung *et al.*, "Large-signal analog modulation response of monolithic optical injection-locked DFB lasers," in *Proc. Conf. Lasers Electro-Optics*, Baltimore, MD, 2005, pp. 1025–1027.
- [8] H.-K. Sung, E. K. Lau, and M. C. Wu, "Optical properties and modulation characteristics of ultrastrong injection-locked distributed feedback lasers," *IEEE J. Sel. Topics Quantum Electron.*, vol. 13, no. 5, pp. 1215–1221, Sep/Oct. 2007.
- [9] L. Chrostowski, C. H. Chang, and C. Chang-Hasnain, "Reduction of relative intensity noise and improvement of spur-free dynamic range of an injection locked VCSEL," in *Proc. IEEE LEOS Annu. Meeting Conf.*, Piscataway, NJ, 2003, vol. 2, pp. 706–7.
- [10] M. C. Espana-Boquera and A. Puerta-Notario, "Noise effects in injection locked laser simulation: Phase jumps and associated spectral components," *Electron. Lett.*, vol. 32, no. 9, pp. 818–19, 1996.
- [11] X. Jin and S. L. Chuang, "Relative intensity noise characteristics of injection-locked semiconductor lasers," *Appl. Phys. Lett.*, vol. 77, no. 9, pp. 1250–2, 2000.
- [12] J. M. Liu *et al.*, "Modulation bandwidth, noise, and stability of a semiconductor laser subject to strong injection locking," *IEEE Photon. Technol. Lett.*, vol. 9, no. 10, pp. 1325–7, Oct. 1997.
- [13] F. Mogensen, H. Olesen, and G. Jacobsen, "FM noise suppression and linewidth reduction in an injection-locked semiconductor laser," *Electron. Lett.*, vol. 21, no. 16, pp. 696–7, 1985.
- [14] K. Schunk *et al.*, "Noise characteristics of injection locked semiconductor lasers," in *Proc. IOOC-ECOC*, Genoa, Italy, 1985, vol. 1, pp. 717–20.
- [15] G. Yabre *et al.*, "Noise characteristics of single-mode semiconductor lasers under external light injection," *IEEE J. Quantum Electron.*, vol. 36, no. 3, pp. 385–93, Mar. 2000.
- [16] X. J. Meng, T. Chau, and M. C. Wu, "Improved intrinsic dynamic distortions in directly modulated semiconductor lasers by optical injection locking," *IEEE Trans. Microw. Theory Tech.*, vol. 47, no. 7, pp. 1172–1176, Jul. 1999.
- [17] L. Chrostowski, C. Chih-Hao, and C. J. Chang-Hasnain, "Enhancement of dynamic range in 1.55- μm VCSELs using injection locking," *IEEE Photon. Technol. Lett.*, vol. 15, no. 4, pp. 498–500, Apr. 2003.
- [18] J. H. Seo, Y. K. Seo, and W. Y. Choi, "Nonlinear distortion suppression in directly modulated DFB lasers by sidemode optical injection," *Proc. IEEE MTT-S Int. Microw. Symp. Dig.*, vol. 1, pp. 555–558, 2001.
- [19] H. K. Sung *et al.*, "Modulation bandwidth enhancement and nonlinear distortion suppression in directly modulated monolithic injection-locked DFB lasers," in *Proc. IEEE Int. Topical Meeting Microw. Photon.*, 2003, pp. 27–30.
- [20] L. Chrostowski *et al.*, "50 GHz directly modulated injection-locked 1.55 μm VCSELs," in *Proc. Opt. Fiber Commun. Conf.*, 2005, pp. 338–340.
- [21] E. K. Lau, H.-K. Sung, and M. C. Wu, "Ultra-high, 72 GHz resonance frequency and 44 GHz bandwidth of injection-locked 1.55- μm DFB lasers," in *Proc. Opt. Fiber Commun. Conf.*, 2006, p. 3.
- [22] H. L. T. Lee *et al.*, "Bandwidth enhancement and chirp reduction in DBR lasers by strong optical injection," in *Proc. Conf. Lasers Electro-Optics*, Salem, MA, 2000, pp. 99–100.
- [23] S. K. Hwang, J. M. Liu, and J. K. White, "35-GHz modulation bandwidth in injection-locked semiconductor lasers," in *Proc. Annu. Meeting IEEE Lasers Electro-Optics Soc.*, 2003, vol. 2, pp. 710–711.
- [24] S. Wiczorek *et al.*, "Improved semiconductor-laser dynamics from induced population pulsation," *IEEE J. Quantum Electron.*, vol. 42, no. 6, pp. 552–562, Jun. 2006.
- [25] F. Mogensen, H. Olesen, and G. Jacobsen, "Locking conditions and stability properties for a semiconductor laser with external light injection," *IEEE J. Quantum Electron.*, vol. QE-21, no. 7, pp. 784–93, Jul. 1985.
- [26] C. H. Henry, N. A. Olsson, and N. K. Dutta, "Locking range and stability of injection locked 1.54 μm InGaAsP semiconductor lasers," *IEEE J. Quantum Electron.*, vol. QE-21, no. 8, pp. 1152–6, Aug. 1985.
- [27] R. Lang, "Injection locking properties of a semiconductor laser," *IEEE J. Quantum Electron.*, vol. QE-18, no. 6, pp. 976–83, Jun. 1982.
- [28] A. Murakami, K. Kawashima, and K. Atsuki, "Cavity resonance shift and bandwidth enhancement in semiconductor lasers with strong light injection," *IEEE J. Quantum Electron.*, vol. 39, no. 10, pp. 1196–204, Oct. 2003.
- [29] T. B. Simpson *et al.*, "Nonlinear dynamics induced by external optical injection in semiconductor lasers," *Quantum Semiclass. Opt.*, vol. 9, pp. 765–84, 1997.
- [30] V. Annovazzi-Lodi *et al.*, "Dynamic behavior and locking of a semiconductor laser subjected to external injection," *IEEE J. Quantum Electron.*, vol. 34, no. 12, pp. 2350–2357, Dec. 1998.
- [31] A. Murakami, "Phase locking and chaos synchronization in injection-locked semiconductor lasers," *IEEE J. Quantum Electron.*, vol. 39, no. 3, pp. 438–47, Mar. 2003.
- [32] T. B. Simpson, J. M. Liu, and A. Gavrielides, "Bandwidth enhancement and broadband noise reduction in injection-locked semiconductor lasers," *IEEE Photon. Technol. Lett.*, vol. 7, no. 7, pp. 709–11, Jul. 1995.
- [33] H.-K. Sung *et al.*, "Optical generation of millimeter-waves using monolithic sideband injection locking of a two-section DFB laser," in *Proc. Conf. Lasers Electro-Optics Soc.*, 2003, vol. 2, pp. 1005–1006.
- [34] E. K. Lau, H. K. Sung, and M. C. Wu, "Frequency response measurement of opto-electronic devices using an optical heterodyne down-conversion technique," , submitted for publication.



Erwin K. Lau (S'01–M'06) received the B.S. and M.Eng. degrees in electrical engineering from the Massachusetts Institute of Technology, Cambridge, in 2000 and 2001, respectively, and the Ph.D. degree in electrical engineering and computer sciences from the University of California, Berkeley, in 2006.

In 2004, he spent a summer at the IBM Thomas J. Watson Research Center, Yorktown, NY where he worked on noise of parallel digital optical interconnects. He is currently a Postdoctoral Researcher in electrical engineering at the University of California,

Berkeley. His research interests are on optical injection locking of semiconductor lasers and high-speed optical communications.



Hyuk-Kee Sung (S'01–M'06) received the B.S. and M.S. degrees in electrical and electronic engineering from Yonsei University, Seoul, Korea, in 1999 and 2001, respectively, and the Ph.D. degree in electrical engineering and computer sciences from the University of California, Berkeley, in 2006.

He is now with the Electronic and Electrical Engineering Department, Hongik University, Seoul, Korea. His research interests are in the area of high-speed optoelectronics including optical injection locking of semiconductor lasers, RF photonics, optoelectronic oscillators, and optical communications.



Ming C. Wu (S'82–M'83–SM'00–F'02) received the B.S. degree in electrical engineering from National Taiwan University, Taipei, Taiwan, R.O.C., and the M.S. and Ph.D. degrees in electrical engineering and computer science from the University of California, Berkeley, in 1985 and 1988, respectively.

From 1988 to 1992, he was a Member of Technical Staff at AT&T Bell Laboratories, Murray Hill, NJ. From 1992 to 2004, he was a Professor in the electrical engineering Department, University of California, Los Angeles, where he also served as Vice

Chair for Industrial Affiliate Program and Director of Nanoelectronics Research Facility. In 2004, he moved to the University of California, Berkeley, where he is currently a Professor of electrical engineering and computer sciences. He is also a Co-Director of Berkeley Sensor and Actuator Center (BSAC). His research interests include optical MEMS, high-speed semiconductor optoelectronics, nanophotonics, and biophotonics. He has published six book chapters, over 135 journal papers and 280 conference papers. He is the holder of 14 U.S. patents.

Prof. Wu is a member of Optical Society of America. He was a Packard Foundation Fellow from 1992 to 1997. He is the founding Co-Chair of IEEE/LEOS Summer Topical Meeting on Optical MEMS (1996), the predecessor of IEEE/LEOS International Conference on Optical MEMS. He has served in the program committees of many technical conferences, including MEMS, OFC, CLEO, LEOS, MWP, IEDM, DRC, ISSCC; and as Guest Editor of two special issues of IEEE journals on optical MEMS.